mathematics

MDPI

Article

A Derivative Fidelity-Based Total Generalized Variation Method for Image Restoration

Tao Zou, Guozhang Li, Ge Ma *, Zhijia Zhao and Zhifu Li

School of Mechanical and Electrical Engineering, Guangzhou University, Guangzhou 510006, China
* Correspondence: m_ge@gzhu.edu.cn

Abstract: Image edge is the most indicative feature that forms a significant role in image analysis and image understanding, but edge-detail preservation is a difficult task in image restoration due to noise and blur during imaging. The balance between edge preservation and noise removal has always been a difficult problem in image restoration. This paper proposes a derivative fidelity-based total generalized variation method (D-TGV) to improve this balance. First, an objective function model that highlights the ability to maintain details is proposed for the image restoration problem, which is combined with a fidelity term in derivative space and a total generalized variation regularization term. This is designed to achieve the advantage of preserving details in derivative space and eliminate the staircase effect caused by traditional total variation. Second, the alternating direction method of the multipliers (ADMM) is used to solve the model equations by decomposing the original, highly complex model into several simple sub-problems to attain rapid convergence. Finally, a series of experiments conducted on standard grayscale images showed that the proposed method exhibited a good balance between detail preservation and denoising but also reached completion with the fewest iterations compared with the currently established methods.

Keywords: derivative space; total generalized variation; image restoration

MSC: 68U10; 94A08

check for updates

Citation: Zou, T.; Li, G.; Ma, G.; Zhao, Z.; Li, Z. A Derivative Fidelity-Based Total Generalized Variation Method for Image Restoration. *Mathematics* **2022**, *10*, 3942. https://doi.org/10.3390/math10213942

Academic Editor: Radu Tudor Ionescu

Received: 19 September 2022
Accepted: 20 October 2022
Published: 24 October 2022

Publisher's Note: MDPI stays neutral with regard to jurisdictional claims in published maps and institutional affiliations.

Copyright: © 2022 by the authors. Licensee MDPI, Basel, Switzerland. This article is an open access article distributed under the terms and conditions of the Creative Commons Attribution (CC BY) license (https://creativecommons.org/licenses/by/4.0/).

1. Introduction

Degraded images may affect the accuracy of image detection and image classification [1,2]. Image restoration obtains original clean images from observed ones according to the following image degradation module:

$$y = Hu + n, \tag{1}$$

where $u \in R^{N\times N}$ is the original image, $y \in R^{N\times N}$ is the observed image, $n \in R^{N\times N}$ is the Gaussian white noise with zero mean and variance σ^2, and $H \in R^{N\times N}$ is the matrix operator that models the acquisition processing. Since H is generally an ill-conditioned operator [3,4] that is short of sufficient constraints; knowing how to recovery the clear image u from its degraded observation y becomes an ill-posed problem that has discomfort characteristics in solution searching. Regularized image restoration methods based on prior knowledge have been widely generalized for alleviating such drawbacks, which can be described as follows:

$$\min_u \Phi(u) + \frac{\mu}{2}\|Hu - y\|_2^2, \tag{2}$$

where $\|Hu - y\|_2^2$ is the fidelity term and $\Phi(u)$ is the regularization term. The term μ is a regularization parameter that balances the relative weight between the fidelity and the regularization terms. Formula (2) is a general formula for image restoration.

Classic regularization models include Tikhonov, ℓ_1-norm, and TV regularization. The earliest Tikhonov regularization model was proposed in [5], which adopted the

quadratic penalty method to guarantee sufficient constraints. Because the function in (2) is both simple and easily computable, Tikhonov regularization is widely used, but there are problems of excessive smoothness and failure to save key secondary details. ℓ_1 regularization [6] uses $\Phi(u) = \|u\|_1$, which is the sum matrix of the absolute values of each element in the image. The presence of the ℓ_1 term encourages small components of u to become exactly zero, generating sparse solutions. It is more about image processing problems where sparseness is sought, such as famous basis pursuit denoising [7], the least absolute shrinkage and selection operator (LASSO) [8], and wavelet-based sparse reconstruction [9]. Rudin et al. introduced the classical total variation (TV) regularization method [10], which is isotropic and has the drawback of over-smoothing. Further research on anisotropic total variation (ATV) [11,12] found that it can preserve the edge of the images but can still produce certain staircase effects in smooth areas, which left a challenging task of texture image restoration. Especially, Ref. [12] proposed an adaptive parameter-estimation method for total variation image restoration (APE-TV), resulting in superiority in speed and competitiveness in accuracy. To further guarantee high-quality restoration, researchers have proposed improved regularization models based on total variation [13–16]. For example, Lysaker proposed a new variational model based on using a second-order difference equation to deal with the problem of the restoration of medical magnetic resonance images [15]. Furthermore, Deng proposed a high-order total variation (HOTV) model [16] that used a regularization term based on higher-order differences in the total variation model. Although these two models can effectively suppress the staircase effect, the image edge details are still affected by over-smoothing. In particular, Bredies et al. combined the first-order gradient with the second-order gradient to propose the total generalized variation regularization method (TGV) [17], which not only suppresses the staircase effect but also can effectively preserve the edge information of the image. He et al. proposed an adaptive total generalized variation model (APE-TGV) [18], which maintains the characteristics of the TGV model while preserving a high level of detail.

Although the above regularization models achieved good effects, they did not perform adequately overall in terms of high-quality restoration for the edge feature, especially for texture images. Because the fidelity term is the traditional error between the solution and original image, it ignores the relationship between detailed structures, resulting in an insufficiently accurate solution of edge details. Therefore, in order to improve these problems, some researchers have improved the fidelity term, for example, through the iterative denoising and back-projection (IDBP) [19] algorithm, which builds fidelity terms by relaxing the effective feasible set in the problem (2), to obtain better image restoration results. At the same time, based on the fact that derivative space [20] has a better ability to protect details, Ref. [21] proposes a method of image restoration based on derivative space (D-ADMM). The algorithm can protect image details and reduce computational time. However, the regularization term of D-ADMM uses the TV regularization, so the staircase effect is unavoidable.

Each above regularized image restoration model involves a complex objective function, which can be solved under split framework efficiently. Typical algorithms for solving TV and TGV models include Split Bregman [22,23], the augmented Lagrange method (ALM) [24], and the alternating direction method of multipliers (ADMM) [25,26]. The ADMM algorithm is an effective method to solve large-scale convex optimization problems with separable structures, which decomposed the original complex problem into several sub-problems. At the same time, the ADMM algorithm allows one to plug in any off-the-shelf image denoisers to solve the sub-problems [27], such as BM3D [28], non-local means (NLM) [29], and deep-learning-based denoisers [30,31]. The BM3D denoiser was used to carry out IDBP, which can make full use of the powerful denoising ability of BM3D. Valsesia et al. [32] proposed to remove noise from images by employing graph-neural networks (GNN). Regarding the deblurring problem, Nah [33] used the generated antagonistic network (GAN) to restore blurred images. Although these denoisers can achieve good

denoising results, it was found that the image could easily become over-smoothed and that the process was time-consuming.

Therefore, considering the ability to maintain details without sacrificing computing speed, this paper proposes a derivative fidelity-based total generalized variation method (D-TGV) for image restoration. The following aspects of the present research are highlighted:

(1) The research proposes an objective function model that highlights the ability to overcome the difficult trade-off between edge preservation and noise removal in image restoration. This is designed to achieve the advantage of preserving details in derivative space and eliminate the staircase effect caused by traditional total variation denoising.
(2) The ADMM algorithm is adopted to solve the proposed model, which can decompose the optimization problem into several separate sub-problems for efficient computation.
(3) In a series of experiments, the proposed method can achieve a good balance between detail preservation and denoising, with the fewest iterations.

In this paper, the method is developed and presented as follows. Section 2 describes the detailed derivation of D-ADMM. Section 3 introduces the whole derivation process of D-TGV. The experimental data of D-TGV are presented in Section 4. Section 5 provides a summary of this paper.

2. Related Work

The TV-based image-restoration problem is as follows:

$$\min_u \frac{\mu}{2}\|Hu - y\|_2^2 + \|Du\|, \tag{3}$$

where $D = \left[D_h^T, D_v^T\right]^T$, such as the discrete gradient operator ∇, is defined as follows:

$$\begin{aligned}(D_h u)_{i,j} &= u_{i,j} - u_{i,j-1} \text{ with } u_{i,-1} = u_{i,N-1}\\ (D_v u)_{i,j} &= u_{i,j} - u_{i-1,j} \text{ with } u_{-1,j} = u_{N-1,j}.\end{aligned} \tag{4}$$

So the anisotropic TV is as follows:

$$\text{TV (anisotropic)} = \sum_{i=0}^{N-1}\sum_{j=0}^{N-1}\left(\left|(D_h u)_{i,j}\right| + \left|(D_v u)_{i,j}\right|\right). \tag{5}$$

Additionally, the isotropic TV is as follows:

$$\text{TV (isotropic)} = \sum_{i=0}^{N-1}\sum_{j=0}^{N-1}\left(\sqrt{(D_h u)_{ij}^2} + \sqrt{(D_v u)_{ij}^2}\right). \tag{6}$$

The augmented Lagrangian method (ALM) can be used to deal with problem (3). Let $x = Hu - y$, $d = Du$, and (3) becomes a constrained problem (7):

$$\begin{aligned}&\min_{u,x,d} \frac{\mu}{2}\|x\|_2^2 + \|d\|,\\ &s.t. \quad x = Hu - y, d = Du.\end{aligned} \tag{7}$$

Introducing $\lambda_1 \in R^N, \lambda_2 \in R^N$ as the Lagrange multiplier, the constrained expression (7) is transformed into an unconstrained problem:

$$\begin{aligned}\Phi(u, x, d, \lambda_1, \lambda_2) = \frac{\mu}{2}\|x\|_2^2 + \|d\| + \lambda_1^T(d - Du) + \frac{\delta}{2}\|d - Du\|_2^2\\ +\lambda_2^T(x - Hu + y) + \frac{\delta}{2}\|x - Hu + y\|_2^2,\end{aligned} \tag{8}$$

where $\delta > 0$ is the ALM penalty parameter.

The solution process is as follows:

$$\left(u^{t+1}, x^{t+1}, d^{t+1}\right) = \arg\min_{u,x,d} \Phi\left(u, x, d, \lambda_1^t, \lambda_2^t\right), \tag{9}$$

$$\lambda_1^{t+1} = \lambda_1^t + \delta\left(d^{t+1} - Du^{t+1}\right), \tag{10}$$

$$\lambda_2^{t+1} = \lambda_2^t + \delta\left(x^{t+1} - Hu^{t+1} + y^{t+1}\right). \tag{11}$$

Note that variables u, x, and d in ALM are iterated in parallel, which is not flexible for computation. Alternatively, the computation of x and d is a natural strategy, denoting an alternating direction method of multipliers (ADMM), which is employed in this paper for achieving rapid convergence.

On the other hand, in order to further improve the quality of the image restoration, derivative space [23] containing more specific information of images can be employed to establish the fidelity term, denoting a white Gaussian noise distribution of random variable $e \in R^{N\times N}$ with mean 0 and covariance σ^2, i.e., $e \sim \mathcal{N}(0, \sigma^2 I)$. Matrix $s \in R^{N\times N}$ is a random variable with a Gaussian distribution $se \sim \mathcal{N}(0, s\sigma^2 s^T)$. Therefore, for the gradient operator D, $De(e = Hu - y)$ is a random variable, $De \sim \mathcal{N}(0, \sigma^2 DD^T)$. Let $d = Du$ ($d = [d_h, d_v] = [D_h u, D_v u]$). Based on the definition of the covariance matrix and the condition of independent, identically distributed random variables, the fidelity term based on the derivative space [21] can be obtained as follows:

$$\|D(Hu - y)\|_2^2 \approx 4\|Hu - y\|_2^2 \ \ s.t. \ \ D_h^T d_v = D_v^T d_h. \tag{12}$$

Because of the inter-change property of the convolution operators, the fidelity term $\|D(Hu - y)\|_2^2$ can be obtained as $\|Hd - Dy\|_2^2$.

3. A Derivative Fidelity-Based Total Generalized Variation Method for Image Restoration

To overcome the difficult trade-off between edge preservation and noise smoothing, as well as the staircase effect, this paper proposes a derivative fidelity-based total generalized variation method for image restoration. The specific model is as follows:

$$\min_{d,p} \alpha_0 \|\varepsilon(p)\|_1 \ + \ \alpha_1 \|d - p\|_1 + \ \frac{\mu}{2}\|Hd - Dy\|_2^2$$

$$s.t. \quad D_h^T d_v = D_v^T d_h. \tag{13}$$

where $p = [p_h, p_v]$ is a two-dimensional first-order tensor, and $\alpha_0 > 0$ and $\alpha_1 > 0$ are positive parameters. For $\varepsilon(p)$, this is expressed as follows:

$$\varepsilon(p) = \begin{bmatrix} D_h p_h & \frac{(D_h p_v + D_v p_h)}{2} \\ \frac{(D_h p_v + D_v p_h)}{2} & D_v p_v \end{bmatrix}. \tag{14}$$

This objective function includes a fidelity term in derivative space that uses the effectiveness of the gradient for edge-detail preservation during image denoising and deblurring, while TGV regularization suppresses the staircase effect. Thus, this model maintains a balance between preserving details and achieving noise removal.

For solving this problem with good computational speed, the ADMM algorithm was used to decompose the optimization problem into several separate sub-problems.

First, let $z = d - p$ and $w = \varepsilon(p)$; then, (13) can be transformed into a constrained problem

$$\min_{d,p,z,w} \quad \alpha_0 \|w\|_1 \ + \ \alpha_1 \|z\|_1 + \ \tfrac{\mu}{2}\|Hd - Dy\|_2^2$$

$$s.t. \quad D_h^T d_v = D_v^T d_h, \ z = d - p, \ w = \varepsilon(p). \tag{15}$$

Secondly, by introducing the variables m_1, m_2 and q, the above problem (15) is transformed into the following unconstrained problem (16):

$$\Phi(d, w, z, m_1, m_2, q) = \alpha_0\|w\|_1 + \alpha_1\|z\|_1 + \frac{\mu}{2}\|Hd - Dy\|_2^2 + \frac{\delta_1}{2}\left\|D_h^T d_v - D_v^T d_h + m_1\right\|_2^2 + \frac{\delta_2}{2}\|w - \varepsilon(p) + q\|_2^2 + \frac{\delta_3}{2}\|z - d + p + m_2\|_2^2, \tag{16}$$

where $\delta_1 > 0$, $\delta_2 > 0$ and $\delta_3 > 0$ are penalty parameters. According to d, p and $\varepsilon(p)$, the following can be be obtained using $q = \begin{bmatrix} q_1 & q_3 \\ q_3 & q_2 \end{bmatrix}, w = \begin{bmatrix} w_1 & w_3 \\ w_3 & w_2 \end{bmatrix}, z = [z_h, z_v]$, and $m_2 = [m_{2,1}, m_{2,2}]$.

Clearly, this is a multivariable optimization problem composed of multiple functions, which can be decomposed into several simple subproblems for computation in the following steps.

Step 1: Computation of d.

$$\min_d \frac{\mu}{2}\|Hd - Dy\|_2^2 + \frac{\delta_1}{2}\left\|D_h^T d_v - D_v^T d_h + m_1\right\|_2^2 + \frac{\delta_3}{2}\|z - d + p + m_2\|_2^2. \tag{17}$$

This is a typical quadratic optimization problem, and the fast Fourier transform is a common method for solving (17). Using periodic boundary conditions, the coefficient matrix can be diagonalized in the Fourier domain. This greatly reduces the computational burden and avoids a large number of numerical calculations due to the large fuzzy matrix. The results are as follows:

$$\begin{aligned} d_h = {} & \mathcal{F}^{-1}(\mathcal{F}(\mu H^T D_h y + \delta_3(z_h + m_{2,1} + p_h) \\ & + \delta_1 D_v(D_h^T d_v + m_1)) \oslash \mathcal{F}(E_h)), \end{aligned} \tag{18}$$

Suppose $\mathcal{F}$ stands for the Fourier transform, $E_h = \mu H^T H + \delta_3 I + \delta_1 D_v D_v^T$, and $\oslash$ indicates the entry-wise division.

At the same time, the following results can be obtained:

$$\begin{aligned} d_v = {} & \mathcal{F}^{-1}(\mathcal{F}(\mu H^T D_v y + \delta_3(z_v + m_{2,2} + p_v) \\ & + \delta_1 D_h(D_v^T d_h - m_1)) \oslash \mathcal{F}(E_v)), \end{aligned} \tag{19}$$

where $E_v = \mu H^T H + \delta_3 I + \delta_1 D_h D_h^T$.

Step 2: Computation of p.

$$\min_p \frac{\delta_2}{2}\|w - \varepsilon(p) + q\|^2 + \frac{\delta_3}{2}\|z - d + p + m_2\|_2^2. \tag{20}$$

This is a quadratic function optimization problem of $p = [p_h, p_v]$, which can be solved by using (21) and (22)

$$\begin{aligned} & \left(\delta_3 I + \delta_2 {D_h}^T D_h + \tfrac{\delta_2}{2} {D_v}^T D_v\right) p_h = \delta_2 [{D_h}^T (w_1 + q_1) \\ & + {D_v}^T \left(w_3 - \tfrac{1}{2} D_h p_v + q_3\right)] - \delta_3 (z_h - d_h + m_{2,1}). \end{aligned} \tag{21}$$

Similarly, the following results of p_v can be obtained by

$$\begin{aligned} & \left(\delta_3 I + \delta_2 {D_v}^T D_v + \tfrac{\delta_2}{2} {D_h}^T D_h\right) p_v = \delta_2 [{D_v}^T (w_2 + q_2) \\ & + {D_h}^T \left(w_3 - \tfrac{1}{2} D_v p_h + q_3\right)] - \delta_3 (z_v - d_v + m_{2,2}). \end{aligned} \tag{22}$$

Step 3: computation of w.

$$\min_{w} \alpha_0 \|w\|_1 + \frac{\delta_2}{2}\|w - \varepsilon(p) + q\|_2^2. \tag{23}$$

This is a typical $\ell_2 - \ell_1$ denoising problem [6], which can be solved directly by the soft threshold method using (24)

$$w = \max\left\{\|\varepsilon(p) - q\|_2 - \frac{\alpha_0}{\delta_2}, 0\right\} \times \frac{\varepsilon(p) - q}{\|\varepsilon(p) - q\|_2}. \tag{24}$$

Step 4: the subproblem of z is also can be solved by soft threshold method as follows:

$$\min_{z} \alpha_1 \|z\|_1 + \frac{\delta_3}{2}\|z - d + p + m_2\|_2^2. \tag{25}$$

and

$$z = \max\left\{\|d - p - m_2\|_2 - \frac{\alpha_1}{\delta_3}, 0\right\} \times \frac{d - p - m_2}{\|d - p - m_2)\|_2}. \tag{26}$$

Step 5: update m_1, m_2 and q.

$$m_1^{t+1} = m_1^t + \gamma(D_h^T d_v^{t+1} - D_v^T d_h^{t+1}) \tag{27}$$

$$m_2^{t+1} = m_2^t + \gamma\left(z^{t+1} - d^{t+1} + p^{t+1}\right) \tag{28}$$

$$q^{t+1} = q^t + \gamma(w^{t+1} - \varepsilon(p^{t+1})), \tag{29}$$

where constant $\gamma > 0$ is step length.

Finally, we have $u = \Gamma(d)$ [21].

The above is the whole solution process. See Algorithm 1 for the algorithm process.

Algorithm 1: D-TGV

Preprocessing $\overline{y} = mean(y)$

Initialize d^0, p^0, q^0, w^0, z^0, m_1^0, m_2^0, set $\mu, \delta_1, \delta_2, \delta_3, \gamma > 0$.

Precompute

$$\mathcal{F}(E_h) = \mathcal{F}\left(\mu A^T A + \delta_3 I + \delta_1 D_v D_v^T\right)$$
$$\mathcal{F}(E_v) = \mathcal{F}\left(\mu A^T A + \delta_3 I + \delta_1 D_h D_h^T\right)$$

while *not converged* **do**

  Compute d^{t+1} *according to* (18) *and* (19);

  Compute p^{t+1} *according to* (21) *and* (22) ;

  Compute w^{t+1} *according to* (24);

  Compute z^{t+1} *according to* (26);

  $m_1^{t+1} = m_1^t + \gamma\left(D_h^T d_v^{t+1} - D_v^T d_h^{t+1}\right)$;

  $m_2^{t+1} = m_2^t + \gamma\left(z^{t+1} - d^{t+1} + p^{t+1}\right)$;

  $q^{t+1} = q^t + \gamma\left(w^{t+1} - \varepsilon\left(p^{t+1}\right)\right)$;

  $t = t + 1$;

end

$u = \Gamma(d)$;

$u = u + \overline{y}$.

4. Results

In this section, a series of experiments using standard grayscale images were employed to verify the effectiveness of the proposed method. The competitive methods APE-TV [12], APE-TGV [18], IDBP [19], and D-ADMM [21] were used for comparison with the proposed approach (for ADMM, the methods containing anisotropy and isotropy are referred to in this discussion as D-ADMM(a) and D-ADMM(i) respectively.). The selected parameter values for the proposed algorithm were $\delta_1 = 4, \delta_2 = 3, \delta_3 = 3, \alpha_0 = 1.618$ and $\alpha_1 = 0.1$. All of the computations were performed in MATLAB 2020a on a PC with an Intel Core (TM) i7-6500U CPU at 2.50 GHz and 8 GB of RAM. The stop criterion was $\frac{\|u^{t+1}-u^t\|}{\|u^t\|} \leq 10^{-4}$, where u^t is the restored result at the tth iteration.

For standard grayscale images, a camera shake kernel [21] with $k = 7$ and additive Gaussian noise with a mean value of 0 and the standard deviation $\sigma = 1 \times 10^{-3}$ were employed to obtain degraded Lena, Banoon, Cameraman, and Building. According to the noise and the actual experimental adjustment, it was found that the parameter $\mu = 1500$ is the best. Original, degraded, and different restored images and their corresponding enlarged details are shown in Figures 1–4. As shown in Figure 1c, the key details after the IDBP algorithm restoration were markedly deteriorated. It can be seen from Figure 1h that the D-TGV method had the best detail-protection ability. Figures 2 and 3 further demonstrate this point. It can be seen from the enlarged view of Figure 3 that D-TGV preserved the finger details the best, while IDBP erases some of the finger details. It can be seen from Figure 4 that D-TGV maintains the brick texture best.

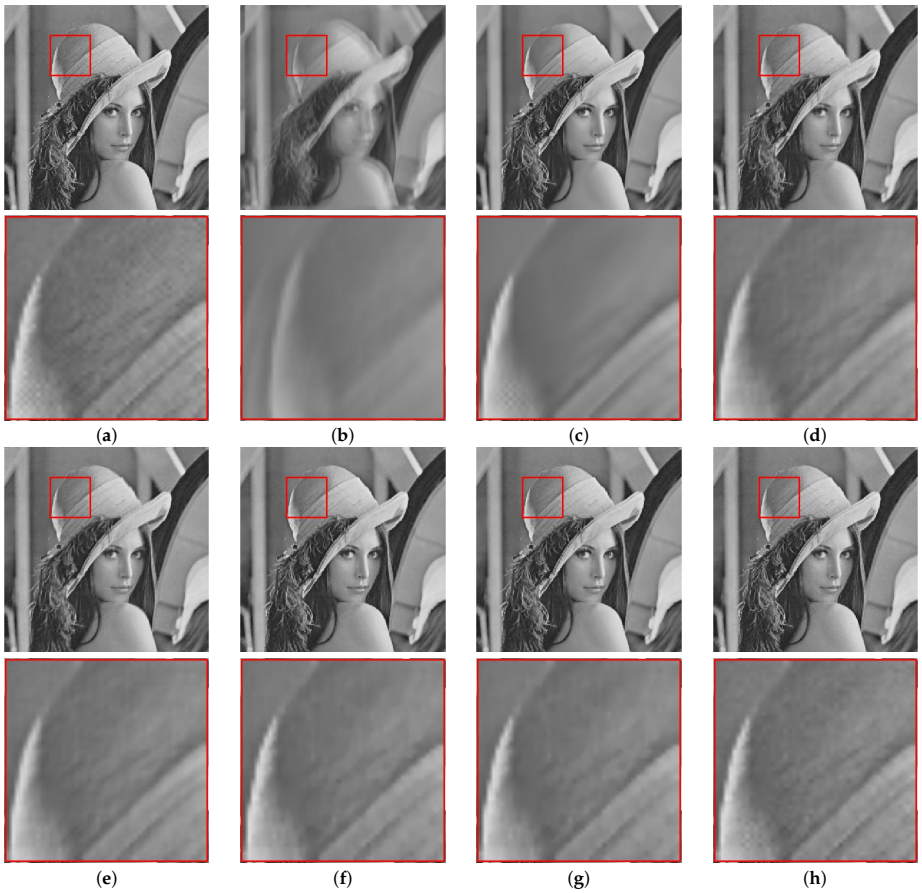

Figure 1. The Lena image restored by all algorithms. (**a**) Lena, (**b**) degraded, (**c**) IDBP, (**d**) D-ADMM(a), (**e**) D-ADMM(i), (**f**) APE-TV, (**g**) APE-TGV, and (**h**) D-TGV.

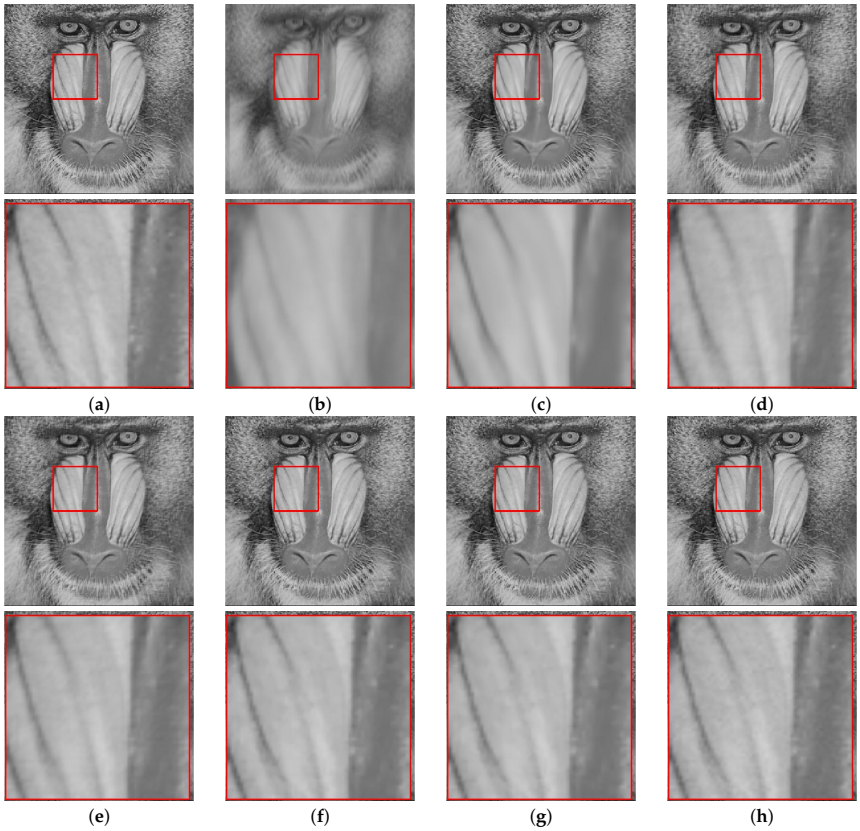

Figure 2. The Banoon image restored by all algorithms. (**a**) Banoon, (**b**) degraded, (**c**) IDBP, (**d**) D-ADMM(a), (**e**) D-ADMM(i), (**f**) APE-TV, (**g**) APE-TGV, and (**h**) D-TGV.

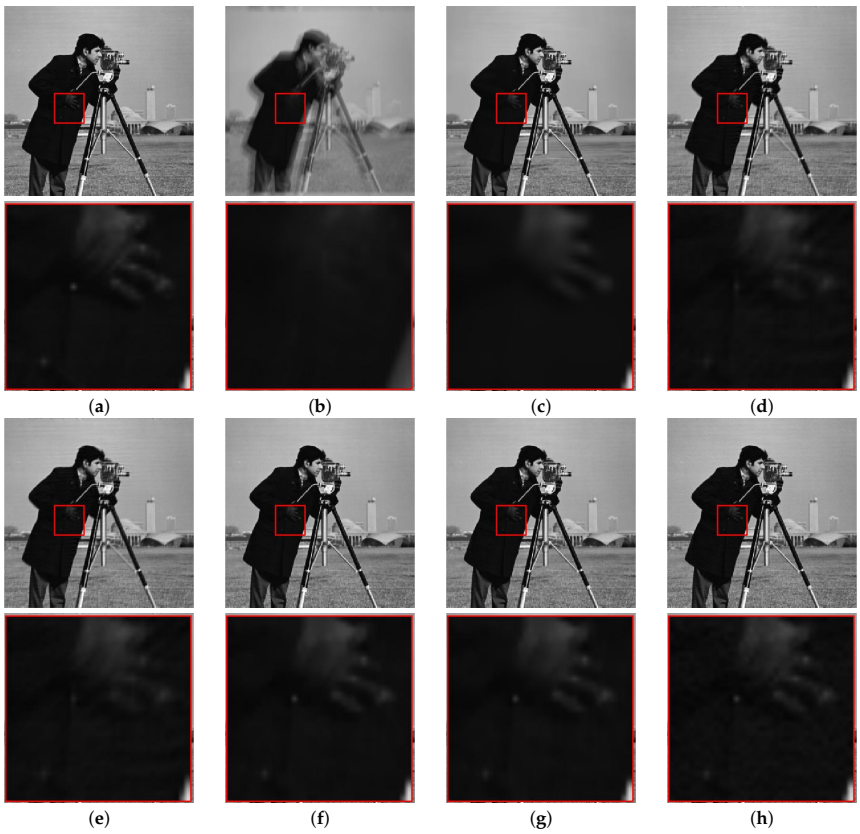

Figure 3. The cameramen image restored by all algorithms. (**a**) Cameramen, (**b**) degraded, (**c**) IDBP, (**d**) D-ADMM(a), (**e**) D-ADMM(i), (**f**) APE-TV, (**g**) APE-TGV, and (**h**) D-TGV.

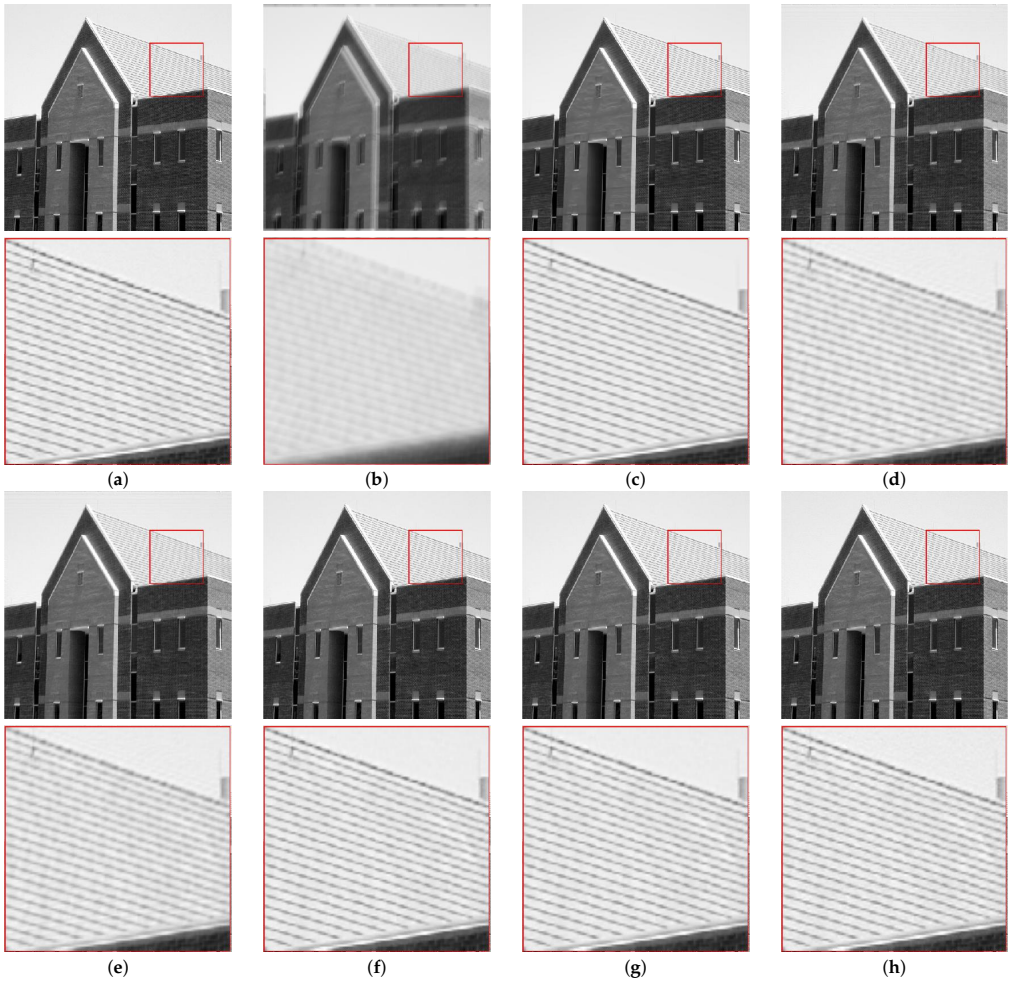

Figure 4. The building image restored by all algorithms. (**a**) Building, (**b**) degraded, (**c**) IDBP, (**d**) D-ADMM(a), (**e**) D-ADMM(i), (**f**) APE-TV, (**g**) APE-TGV, and (**h**) D-TGV.

Figures 5 and 6 show the iteration-variance of MSE and PSNR. It can be seen that the D-TGV algorithm had the lowest MSE, the best PSNR, and the fewest iterations. The detailed values are shown in Table 1.

Table 1 shows the experimental results of several observations degraded by different sizes of blur kernels, including the objective indicators PSNR and SSIM, and the total iterations. For all experiments, D-TGV obtained the best PSNR and better SSIM, representing a balance between the denoising effect and detail-retention ability. In particular, the number of iterations of the proposed method was less than half of that of the comparison algorithm, which clearly represented a significant processing advantage.

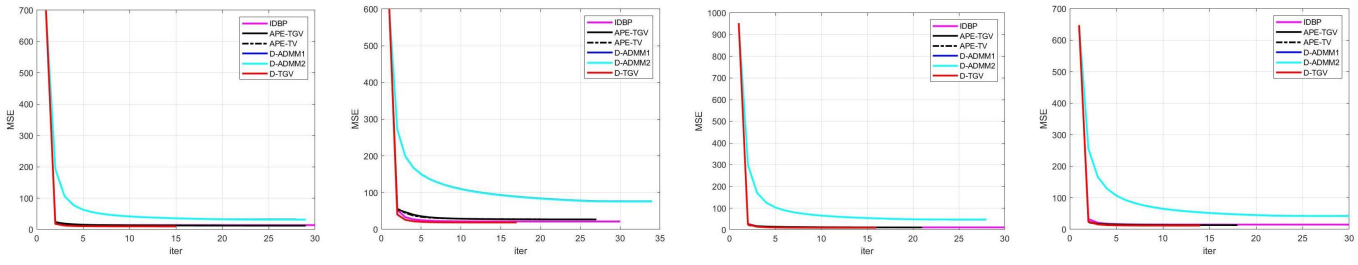

Figure 5. Iteration-varying of MSE. (**a**) Lena, (**b**) Banoon, (**c**) cameraman, and (**d**) building.

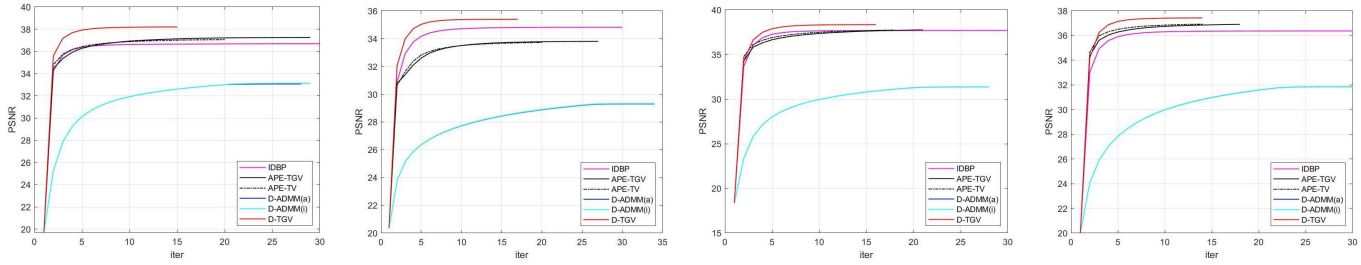

(**a**) (**b**) (**c**) (**d**)

Figure 6. Iteration-varying of PSNR. (**a**) Lena, (**b**) Banoon, (**c**) cameraman, and (**d**) building.

Table 1. Restoration results on PSNR, SSIM, and iterations (Bold fonts denote the best).

		PSNR			SSIM			Iter		
Image	**Name**	**3**	**5**	**7**	**3**	**5**	**7**	**3**	**5**	**7**
Building	IDBP	36.34	36.57	36.37	0.9314	0.934	0.9319	30	30	30
	APE_TGV	37.72	38.65	36.91	0.9601	**0.9652**	**0.9511**	79	82	87
	APE_TV	37.76	38.64	36.94	**0.9604**	0.9651	0.9512	64	66	70
	D-ADMM(a)	32.25	32.83	31.86	0.9189	0.9288	0.9049	32	28	30
	D-ADMM(i)	32.25	32.83	31.87	0.9183	0.9287	0.9049	32	28	30
	D-TGV	**38.16**	**39.17**	**37.43**	0.9547	0.9628	0.9494	**12**	**13**	**14**
Lena	IDBP	36.92	37.03	36.75	0.9337	0.9355	0.9334	30	30	30
	APE_TGV	37.65	38.06	37.27	**0.9592**	0.9644	**0.9581**	123	127	141
	APE_TV	37.44	37.86	37.07	0.9583	0.9636	0.9573	93	94	102
	D-ADMM(a)	33.07	33.45	33.08	0.9341	0.9426	0.9378	32	28	28
	D-ADMM(i)	33.07	33.45	33.13	0.9337	0.9425	0.9382	32	28	29
	D-TGV	**38.49**	**39.18**	**38.21**	0.9583	**0.965**	0.9571	**13**	**14**	**15**
Cameraman	IDBP	38.06	38.35	37.73	0.9537	0.9554	0.952	30	30	30
	APE_TGV	38.24	38.59	37.8	0.968	**0.9716**	0.966	92	93	103
	APE_TV	38.23	38.55	37.78	**0.9683**	0.9715	0.9661	79	80	88
	D-ADMM(a)	31.38	31.5	31.37	0.9321	0.9414	0.9271	31	28	28
	D-ADMM(i)	31.36	31.5	31.36	0.931	0.9407	0.9262	31	28	28
	D-TGV	**38.67**	**39.37**	**38.36**	0.9509	0.9595	0.9508	**14**	**15**	**16**
Banoon	IDBP	35.29	35.87	34.79	0.951	0.9563	0.9475	30	30	30
	APE_TGV	34.67	35.3	33.83	0.9632	0.9699	0.9572	119	114	133
	APE_TV	34.59	35.25	33.74	0.9627	0.9697	0.9566	86	84	92
	D-ADMM(a)	29.73	30.2	29.31	0.9004	0.9139	0.8919	33	30	34
	D-ADMM(i)	29.75	30.21	29.33	0.901	0.9142	0.8925	33	30	34
	D-TGV	**36.33**	**37.15**	**35.41**	**0.9711**	**0.9772**	**0.9667**	**15**	**17**	**17**

5. Conclusions

In this paper, a derivate fidelity-based total generalized variational image restoration method is proposed. This method utilizes the spatial detail preservation ability of gradients and the ability of TGV to suppress the staircase effect, achieving an effective balance between edge-detail preservation and denoising. A series of experiments on standard grayscale images showed that the proposed method was the best for texture protection. At the same time, the proposed algorithm not only obtained the highest PSNR, but also the number of iterations required was less than half of the comparison method. This method focuses on the typical problem of the convex optimization method, in which the regular-

ization is certain. Considering the flexible characteristic of the choice on regularization, deep-learning-based image restoration will be the key point of our further research.

Author Contributions: G.M. and G.L. developed the idea that resulted in this paper and were responsible for the experimental collation; Z.L. contributed to the design of experiments; and Z.Z. and T.Z. contributed to manuscript writing. All authors have read and agreed to the published version of the manuscript.

Funding: This paper is supported by Key-Area Research and Development Program of Guangdong Province (Grant NO. 2020B0101050001), the Science and Technology Planning Project of Guangzhou City (Grant NO. 202102020876, 202102010411), the National Natural Science Foundation of China (Grant NO. 61803110, 52171331).

Institutional Review Board Statement: Not applicable.

Informed Consent Statement: Not applicable.

Data Availability Statement: Not applicable.

Conflicts of Interest: The authors declare no conflict of interest.

References

1. Cheng, J.; Liu, L.; Chen, F.; Jiang, Y. Meaningful Secret Image Sharing with Uniform Image Quality. *Mathematics* **2022**, *10*, 3241. [CrossRef]
2. Wu, H.; Du, C.; Ji, Z.; Gao, M.; He, Z. SORT-YM: An Algorithm of Multi-Object Tracking with YOLOv4-Tiny and Motion Prediction. *Electronics* **2021**, *10*, 2319. [CrossRef]
3. Zhong, M.; Wang, W.; Zhu, K. On the asymptotical regularization with convex constraints for nonlinear ill-posed problems. *Appl. Math. Lett.* **2022**, *133*, 108247. [CrossRef]
4. Tikhonov, A.N.; Goncharsky, A.V.; Stepanov, V.V.; Yagola, A.G. *Numerical Methods for the Solution of Ill-Posed Problems*; Springer Science Business Media: Berlin/Heidelberg, Germany, 1995; p. 328.
5. Tikhonov, A.N.; Arsenin, V.Y. Solutions of ill-posed problems. *Math. Comput.* **1978**, *32*, 1320–1322.
6. Zhuang, Y.; Che, H.; Chen, H. A linearly convergent algorithm without prior knowledge of operator norms for solving $\ell_1 - \ell_2$ minimization. *Appl. Math. Lett.* **2022**, *125*, 107717. [CrossRef]
7. Chen, S.S.; Donoho, D.L.; Saunders, M.A. Atomic Decomposition by Basis Pursuit. *SIAM J. Sci. Comput.* **1998**, *20*, 33–61. [CrossRef]
8. Tibshirani, R. Regression Shrinkage and Selection via the Lasso. *J. R. Stat. Soc. Ser. B Methodol.* **1996**, *58*, 267–288. [CrossRef]
9. Figueiredo, M.A.; Nowak, R.D.; Wright, S. Gradient Projection for Sparse Reconstruction: Application to Compressed Sensing and Other Inverse Problems. *IEEE J. Sel. Top. Signal Process.* **2007**,*1*, 586–597. [CrossRef]
10. Rudin, L.I.; Osher, S.; Fatemi, E. Nonlinear total variation based noise removal algorithms. *Phys. D Nonlinear Phenom.* **1992**, *60*, 259–268. [CrossRef]
11. Esedoğlu, S.; Osher, S.J. Decomposition of images by the anisotropic [CrossRef] rudin-osher-fatemi model. *Commun. Pure Appl. Math.* **2004**, *57*, 1609–1626. [CrossRef]
12. He, C.; Hu, C.; Zhang, W.; Shi, B. A fast adaptive parameter estimation for total variation image restoration. *IEEE Trans. Image Process.* **2014**, *23*, 4954–4967. [CrossRef] [PubMed]
13. Zhao, P.P.; Huang, Y.M. A restrictive preconditioner for the system arising in half-quadratic regularized image restoration. *Appl. Math. Lett.* **2021**, *115*, 106916. [CrossRef]
14. Liu, X.; Huang, L.; Guo, Z. Adaptive fourth-order partial differential equation filter for image denoising. *Appl. Math. Lett.* **2011**, *24*, 1282–1288. [CrossRef]
15. Lysaker, O.M.; Lundervold, A.; Tai, X.C. Noise removal using fourth-order partial differential equation with applications to medical magnetic resonance images in space and time. *IEEE Trans. Image Process.* **2003**, *12*, 1579–1590. [CrossRef] [PubMed]
16. Deng, L.; Fang, Q.; Zhu, H. Image denoising based on spatially adaptive high order total variation model. In Proceedings of the 2016 9th International Congress on Image and Signal Processing, BioMedical Engineering and Informatics (CISP-BMEI), Datong, China, 15–17 October 2016; pp. 212–216.
17. Bredies, K.; Kunisch, K.; Pock, T. Total generalized variation. *SIAM J. Imaging Sci.* **2010**, *3*, 492–526. [CrossRef]
18. He, C.; Hu, C.; Yang, X. An adaptive total generalized variation model with augmented lagrangian method for image denoising. *Math. Probl. Eng.* **2014**, *2014*, 157893. [CrossRef]
19. Tirer, T.; Giryes, R. Image restoration by iterative denoising and backward projections. *IEEE Trans. Image Process.* **2019**, *28*, 1220–1234. [CrossRef]
20. Patel, V.M.; Maleh, R.; Gilbert, A.C.; Chellappa, R. Gradient-based image recovery methods from incomplete Fourier measurements. *IEEE Trans. Image Process.* **2011**, *21*, 94–105. [CrossRef]

21. Ren, D.; Zhang, H.; Zhang, D. Fast total-variation based image restoration based on derivative alternated direction optimization methods. *Neurocomputing* **2015**, *170*, 201–212. [CrossRef]
22. Afonso, M.V.; Bioucas-Dias, J.M.; Figueiredo, M.A. Fast image recovery using variable splitting and constrained optimization. *IEEE Trans. Image Process.* **2010**, *19*, 2345–2356. [CrossRef]
23. Afonso, M.V.; Bioucas-Dias, J.M.; Figueiredo, M.A. An augmented lagrangian approach to the constrained optimization formulation of imaging inverse problems. *IEEE Trans. Image Process.* **2011**, *20*, 681–695. [CrossRef] [PubMed]
24. Li, C.; Wang, C.L.; Wang, J. Convergence analysis of the augmented lagrange multiplier algorithm for a class of matrix compressive recovery. *Appl. Math. Lett.* **2016**, *59*, 12–17. [CrossRef]
25. Jung, Y.M.; Shin, B.; Yun, S. Global attractor and limit points for nonsmooth admm. *Appl. Math. Lett.* **2022**, *128*, 107890. [CrossRef]
26. Davis, D.; Yin, W. Faster convergence rates of relaxed peaceman-rachford and admm under regularity assumptions. *Math. Oper. Res.* **2017**, *42*, 783–805. [CrossRef]
27. Teodoro, A.M.; Bioucas-Dias, J.M.; Figueiredo, M.A. Image restoration and reconstruction using variable splitting and class-adapted image priors. In Proceedings of the 2016 IEEE International Conference on Image Processing (ICIP), Phoenix, AZ, USA, 25–28 September 2016; pp. 3518–3522.
28. Dong, W.; Zhang, L.; Shi, G. Nonlocally centralized sparse representation for image restoration. *IEEE Trans. Image Process.* **2013**, *22*, 1620–1630. [CrossRef]
29. Xiao, Y.H.; Song, H.N. An inexact alternating directions algorithm for constrained total variation regularized compressive sensing problems. *J. Math. Imaging Vis.* **2012**, *44*, 114–127. [CrossRef]
30. Dong, W.; Wang, P.; Yin, W. Denoising prior driven deep neural network for image restoration. *IEEE Trans. Pattern Anal. Mach. Intell.* **2019**, *41*, 2305–2318. [CrossRef]
31. Dou, H.X.; Huang, T.Z.; Zhao, X.L. Semi-blind image deblurring by a proximal alternating minimization method with convergence guarantees. *Appl. Math.Comput.* **2020**, *377*, 125168. [CrossRef]
32. Valsesia, D.; Fracastoro, G.; Magli, E. Image denoising with graph-convolutional neural networks. In Proceedings of the 2019 IEEE International Conference on Image Processing (ICIP), Taipei, Taiwan, 22–25 September 2019; pp. 2399–2403.
33. Nah, S.; Hyun Kim, T.; Mu Lee, K. Deep multi-scale convolutional neural network for dynamic scene deblurring. In Proceedings of the 2017 IEEE Conference on Computer Vision and Pattern Recognition (CVPR), Honolulu, HI, USA, 21–26 July 2017; pp. 3883–3891.